


Article

Optimization of Flat-Rolling Parameters for Thermally Stable Alloy of Al-Cu-Mn System with Micro Additions of Si and Zr

Alexander Koshmin ^{1,2,*} , Stanislav Cherkasov ², Anastasiya Fortuna ³, Yury Gamin ² 
and Alexander Churyumov ⁴ 

¹ Scientific Activity Sector, Moscow Polytechnic University, Bolshaya Semyonovskaya 38, 107023 Moscow, Russia

² Department of Metal Forming, National University of Science and Technology MISIS, Leninsky Prospekt 4, 119049 Moscow, Russia; y.gamin@misis.ru (Y.G.)

³ Department of Physical Materials Science, National University of Science and Technology MISIS, Leninsky Prospekt 4, 119049 Moscow, Russia

⁴ Department of Physical Metallurgy of Non-Ferrous Metals, National University of Science and Technology MISIS, Leninsky Prospekt 4, 119049 Moscow, Russia; churyumov@misis.ru

* Correspondence: koshmin.an@misis.ru

Abstract: The phase composition, microstructure, and mechanical properties of flat-rolled experimental Al-Cu-Mn system alloy with Si and Zr additions have been studied. The experimental results have been compared with data for the AA2219 commercial alloy pertaining to the same alloying system. Hot deformation of an experimental alloy causes the precipitation of ~100 nm sized dispersoids and refinement of the eutectic phase particles. The yield strength and relative elongation of the hot-deformed experimental alloy are 255 MPa and 8.6%, respectively. Subsequent cold deformation reduces the relative elongation by 3.5% and increases the yield strength by 50 MPa, while the ultimate tensile strength does not change. After long-term 350 °C exposure, the mechanical properties of the experimental alloy remain the same as those of the as-deformed one, whereas the yield strength of the 2219 alloy decreases by 2 times and the ultimate tensile strength by 1.4 times. Comparison of these experimental results with data for the 2219 alloy and other Al-Cu-Mn system alloys cited in this work and reported elsewhere suggests that a good thermal stability of Al-2Cu-2Mn-0.4Si-0.2Zr alloy rolled stock can be achieved through treatment using the regimes designed herein.

Keywords: aluminum alloy; Al-Cu-Mn system; deformation; thermostability; microstructure; mechanical properties



Citation: Koshmin, A.; Cherkasov, S.; Fortuna, A.; Gamin, Y.; Churyumov, A. Optimization of Flat-Rolling Parameters for Thermally Stable Alloy of Al-Cu-Mn System with Micro Additions of Si and Zr. *Metals* **2023**, *13*, 2019. <https://doi.org/10.3390/met13122019>

Academic Editor: Frank Czerwinski

Received: 20 November 2023

Revised: 12 December 2023

Accepted: 15 December 2023

Published: 16 December 2023



Copyright: © 2023 by the authors. Licensee MDPI, Basel, Switzerland. This article is an open access article distributed under the terms and conditions of the Creative Commons Attribution (CC BY) license (<https://creativecommons.org/licenses/by/4.0/>).

1. Introduction

Aluminum and its alloys are widely used in a number of branches due to their unique combination of mechanical and physical properties, high processability, and, most importantly, low cost and abundance. Deformable 2xxx series aluminum alloys (Al-Cu and Al-Cu-Mn) have found broad application in the aircraft and spacecraft industries due to the possibility of their long-term operation over a wide temperature range without compromise in performance [1]. The 2219 (Al-6Cu-Mn) alloy of the abovementioned series is still commonly used as a construction material for operation at elevated (up to 315 °C) and cryogenic temperatures [2]. However, high performance of AA2219 alloy products can only be achieved after combined heat and deformation treatment including ingot homogenization, quenching, and aging of deformed semi-finished products [3]. This process route requires strict adherence to the processing parameters, which is difficult to realize in the conditions of large industrial enterprises and their narrow process windows, as it increases the overall time consumption and cost of production and dictates the necessity to use special process equipment. Furthermore, there are indications that the strength of this alloy decreases dramatically at elevated temperatures (above 200 °C) [4,5].

It is well-known that the mechanical properties of the Al-Cu system alloys, including AA2219, depend on the size and morphology of their structural components that are in turn controlled by the Al_2Cu (θ) and $\text{Al}_{20}\text{Cu}_2\text{Mn}_3$ (Al_{20}) phase formation conditions [6,7]. The θ phase forms from the metastable θ' and θ'' as a result of deformation and heat treatment and the decomposition of the supersaturated solid solution, respectively [8–10]. The precipitation of the ternary Al_{20} phase is also a result of 2219 alloy heat treatment, but it occurs mainly at below 450 °C [11,12] which is far lower than the 2219 alloy homogenization temperature. The formation of fine copper- and manganese-containing phases is a necessary factor that provides for good physical and mechanical properties and preserves these properties in the course of high-temperature operation by hindering recrystallization processes [13–16]. Whereas some researchers have focused on the improvement of Al-Cu system alloys' properties by zirconium and scandium alloying [17–21], as well as various rare earth metals like yttrium, erbium, or gadolinium [22–24], others explore the possibility of replacing the graded alloy for non-heat-treatable Al-Cu-Mn system alloys containing less Cu.

Recent publications [11,25,26] have reported on the production of deformed Al-Cu-Mn alloy sheets with Zr and Sc additives. It was shown that acceptable strength and refractory properties can be achieved for alloys containing 1–2% Cu and Mn and up to 0.2% Zr and Sc. The phase composition of these alloys, expressed as $(\text{Al}) + \text{Al}_3(\text{Zr},\text{Sc}) + \text{Al}_{20}$, provides for a high thermal stability and favors θ phase content reduction which is auspicious for the plasticity of the alloys and allows one to exclude the homogenization step from the process route. One should, however, bear in mind the high cost of Sc (up to USD 10 per gram of high-purity metal and up to USD 25 per kilogram of AlSc_2 ligature) generally limiting its use as an alloying additive [27,28]. Other works [29–31] have dealt with the effect of Si and Fe on the phase composition of Al-Cu-Mn alloys after different types of deformation and heat treatment. It was found that small additions of those elements (up to 0.4%) favor the precipitation of the $\text{Al}_{15}(\text{Fe},\text{Mn})_2\text{Si}_3$ (Al_{15}) and $\text{Al}_6(\text{Fe},\text{Mn},\text{Cu})$ (Al_6) phases which decelerate the development of recrystallization processes in the alloy structure during long-term exposure to elevated temperatures. Other data [32] suggest that the presence of silicon in an amount of 0.4% in the alloy is sufficient for the formation of equal fractions of Mn-containing Al_{20} and Al_{15} dispersoids and, probably, their refinement which favors strength improvement.

However, despite the obviously available detailed data on the structure and properties of the Al-Cu-Mn system alloys with a lowered Cu percentage and Si addition in the absence of Fe, there are still insufficiently studied issues, e.g., optimum process routes and processing conditions, including deformation and heat-treatment steps. Furthermore, there is no information on the effect of low-rate cold deformation (up to 50%) on the properties of experimental Al-Cu-Mn system alloys. Thus, it is an important task to study the structure of the non-heat-treatable Al-2%Mn-2%Cu alloy with 0.4% Si and 0.2% Zr additions and the effect of deformation treatment on the performance of the rolled sheets. Another task of this work is to study the effect of cold preliminary deformation on the properties of the aged 2219 type alloy (2219 hereinafter in the work). The main goal of this work is to develop a process route for Al-2%Mn-2%Cu-0.4%Si-0.2Zr alloy sheet rolling and to compare experimental data for that alloy with those for the graded heat-treatable alloy in order to identify potential advantages of the experimental alloy and test the thermal stability of the alloys at 350 °C.

2. Methods and Materials

The charge materials for ingots of the desired composition alloy were high-purity aluminum (99.99%), copper (99.9%) and Al-10%Mn, Al-12%Si and Al-15%Zr alloying additions. The alloys were melted in a PP-10 muffle furnace with fire-clay crucibles. After the complete melting of the charge, the melt was held for 10 min in the crucible and cast into graphite molds at 750 °C to flat 20 × 130 × 180 mm ingots (H × W × L). The ingot-cooling

rate was approx. 20 K/s. Spectral data (Oxford Instruments) suggest a good match between the actual and target chemical compositions (Table 1).

Table 1. Chemical composition of investigated aluminum alloys.

| Alloy | Composition, wt.% | | | | | |
|-------|-------------------|-------------|-------------|-------------|-------------|-------|
| | Al | Cu | Mn | Zr | Si | Fe |
| 2219 | Balance | 6.18 ± 0.09 | 0.37 ± 0.04 | 0.30 ± 0.08 | - | ≤0.01 |
| CMSZ | Balance | 2.03 ± 0.07 | 1.94 ± 0.05 | 0.17 ± 0.08 | 0.41 ± 0.04 | ≤0.01 |

The ingots were rolled in an ambient atmosphere on a two-high SKET mill, equipped with an open-type housing, mechanical gap-setting system, and individual rolls drive. The rolls diameter and length are 210 mm and 300 mm, respectively, and their circumferential speed is 30 rpm. The rolling temperature was varied by heating in a SNOL 8,2/1100 LSM muffle furnace. The ingots were deformed to the target sizes gradually in 10 sequential passes of 10–25% each with intermediate heating between the passes for temperature homogenization to the target value of 400 °C.

The processing modes differed for two test-alloy batches (Table 2). The 2219 alloy ingots before hot deformation were homogenization annealed at 535 °C for 12 h and then rolled in several passes at 400 °C to 2.0, 2.06, and 2.2 mm thick sheets. Part of the 2.0 mm thick sheets were annealed at 410 °C, while other 2.0 mm sheets were exposed to solution treatment at 535 °C for 1 h followed by water quenching and artificial aging at 175 °C for 18 h (according to AMS2770R). Some of the 2.06 and 2.2 mm sheets were additionally cold-rolled between the quenching and aging operations to strain (ϵ) of 3 and 9%, respectively. Cold deformation was conducted no later than 1 h after quenching.

Table 2. Deformation and heat-treatment modes of test Al alloys.

| Alloy | Designation | Thermal and Deformation Processing Route |
|-------|---------------|--|
| 2219 | HR (2219) | HR 2.0 mm |
| | O | HR 2.0 mm, Ann 410 °C-1 h |
| | Q | HR 2.0 mm, Ann 535 °C-1 h, Q |
| | AA | HR 2.0 mm, Ann 535 °C-1 h, Q, AA 175 °C-18 h |
| | AA3 | HR 2.06 mm, Ann 535 °C-1 h, Q, CR 3%, AA 175 °C-18 h |
| | AA9 | HR 2.20 mm, Ann 535 °C-1 h, Q, CR 9%, AA 175 °C-18 h |
| | A350-6 (2219) | HR 2.0 mm, Ann 535 °C-1 h, Q, AA 175 °C-18 h, Ann 350 °C-6 h |
| CMSZ | HR (CMSZ) | HR 2.0 mm |
| | CR25 | HR 2.5 mm, CR 25% |
| | CR33 | HR 3.0 mm, CR 33% |
| | CR50 | HR 4.0 mm, CR 50% |
| | A350-6 (CMSZ) | HR 4.0 mm, CR 50%, Ann 350 °C-6 h |

HR—Hot rolling. CR—Cold rolling. Ann—Annealing. Q—Quenching in water. AA—Artificial Aging.

Due to the proven best processability of the CMSZ alloy [16] the process route for its sheets was far shorter and included 400 °C hot rolling and cold rolling of 2.5, 3.0, and 4.0 mm sheets to ϵ = 25, 33, and 50%, respectively. For evaluating the effect of high-temperature treatment on the structure and properties of the 2219 and CMSZ alloys, the deformed sheets were annealed at 350 °C for 6 h.

The main methods used for characterizing the structure and the mechanical and physical properties of the test alloys were electron microscopy, electrical conductivity measurement, hardness, and tensile tests. The weight fraction of the solid phases and

isothermal section were calculated using the Thermo-Calc 3.1 software (TTAL5 database). The microstructure was studied using scanning electron microscopy (SEM, TESCAN VEGA 3, TESCAN Brno, s.r.o., Brno, Czech Republic) and transmission electron microscopy (TEM, JEOL JEM-1400, JEOL Ltd., Tokyo, Japan), and the phase composition was verified using electron microprobe analysis (EMPA, OXFORD Aztec, Aztec, Oxford, Abingdon, UK). The specimens were prepared for the tests through mechanical treatment on a disc grinder (ATM SAPHIR 560, ATM GmbH, Blieskastel, Germany) and electrolytic treatment in a perchloric acid–ethanol electrolyte at 12 V. TEM foils were made using PIPS (Precision Ion Polishing System, Gatan, Inc., Pleasanton, CA, USA) ion beam thinning. The Vickers (HV) microhardness was measured with a digital hardness tester MH-6 (Metkon Instruments Ltd., Bursa, Turkey) at a 1000 g load with a 10 s dwell time. The electrical conductivity (EC) was measured with an eddy current structroscope (RII-MSIA “Spectrum” VE-26NP). The ultimate tensile strength (UTS), yield strength (YS), and relative elongation (El) tests were carried out on an Instron 5900 Series universal tester at a 0.001 s^{-1} strain rate. The tensile test specimens were taken from the sheets along the rolling direction.

3. Results and Discussion

3.1. Phase Diagram Calculation

The as-crystallized alloys were theoretically analyzed by means of Scheil–Gulliver simulation (Figure 1a). According to the nonequilibrium crystallization curve presented, one should anticipate the formation of Al_{15} and Al_2Cu eutectic phase and Si crystals. The formation of primary Al_6Mn and Al_3Zr phase crystals under the actual crystallization conditions is suppressed by the formation of a manganese- and zirconium-supersaturated aluminum solid solution (Al). Figure 1b shows the isothermal section of the Al–Cu–Mn–0.2Zr–0.4Si system at 350°C : this temperature is accepted as the working one for the new alloy. It can be seen that the composition of the new alloy falls in the four-phase region containing Al_3Zr , Al_{15} and Al_{20} aluminides which should be expected to precipitate in the form of dispersoids during the decomposition of the supersaturated aluminum solid solution. It is the presence of these phases that is anticipated to provide for a highly stable alloy structure at elevated temperatures.

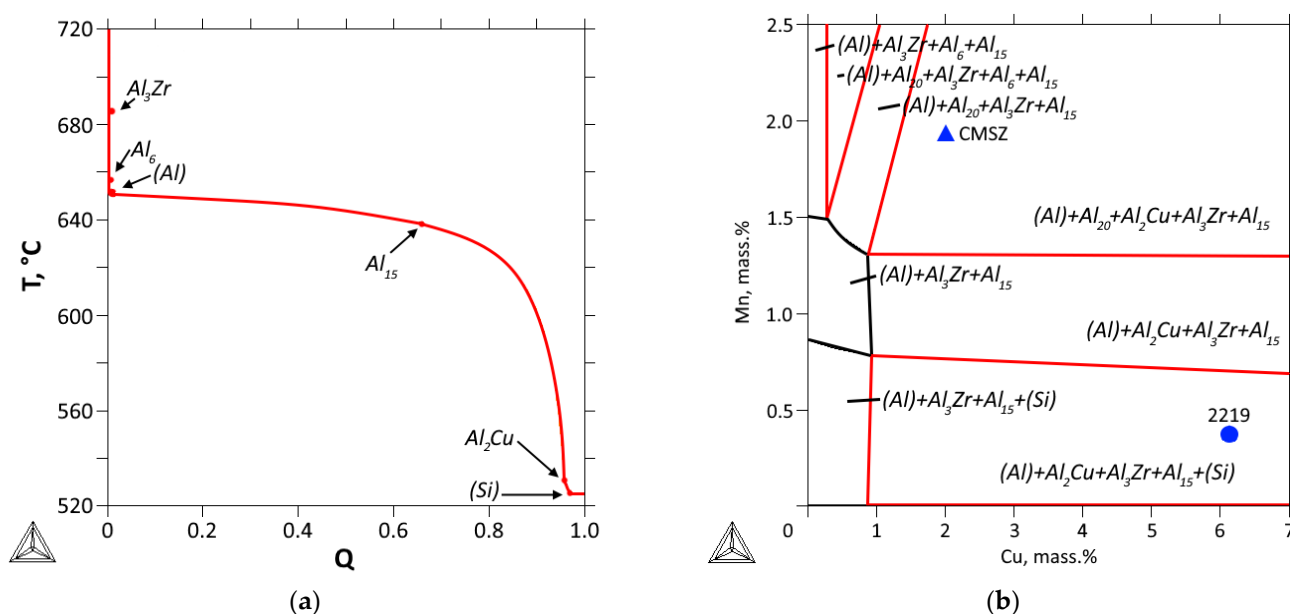


Figure 1. Mole fraction of solid phases (Q) versus temperature (a) and 350°C isothermal section (b) of CMSZ alloy.

3.2. Microstructure

Figure 2 shows microstructural images of 2219 alloy ingots homogenized at 535 °C and as-cast and hot rolled CMSZ alloy ingots. The images clearly show the difference between the microstructures of the test alloys. The microstructural image of the 2219 alloy (Figure 2a) suggests that the Al_2Cu phase did not undergo a complete dissolution since the Cu content is above its solubility limit in Al at the selected homogenization temperature 535 °C. As a result, that phase remained in the structure in the form of spherical particles up to 15 μm in size at dendrite cell boundaries. The slow post-annealing cooling of the alloy favored the precipitation of Cu- and Mn-containing secondary phase crystals.

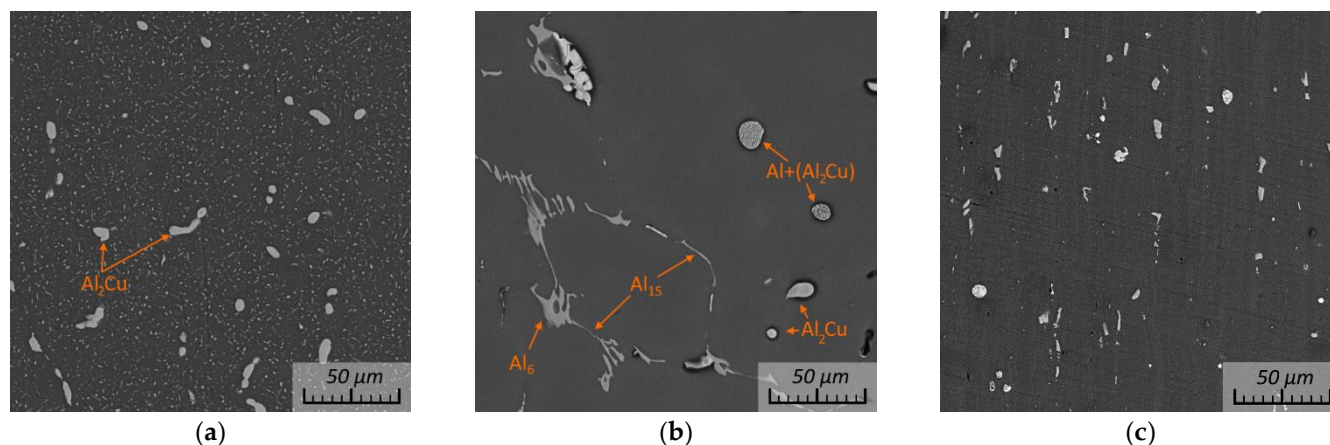


Figure 2. SEM images of experimental alloys: (a) 2219 after homogenization at 535 °C for 12 h, (b) as-cast CMSZ, and (c) HR-CMSZ.

Due to the far smaller Cu content in the CMSZ alloy, its concentration in the structure of the Al_2Cu eutectic phase inclusions was far lower than in the grade alloy. However, an increase in the Mn content in the alloy provided for the precipitation of the crystallization-type manganese-containing eutectic phases. As can be seen from the micrograph, those phases precipitate at the boundaries of (Al) cells in the form of streaks. This difference in the microstructure is expected to improve the mechanical properties and processability of the CMSZ alloy since the refinement of the eutectic phase inclusions during hot rolling at 400 °C followed by cold rolling provides for the formation of fine eutectic phase particles limiting the growth of subgrains at high temperatures and, hence, stabilizing the structure. As can be seen from the micrograph (Figure 2c), hot rolling refined the eutectic phase particles and homogenized their distribution. It can be clearly seen that the particles are arranged in the rolling direction.

Despite the visible refinement and a more homogeneous distribution of the eutectic phase particles as a result of deformation, the main contribution to the thermal stability of the CMSZ alloy pertains to the secondary phase dispersoids forming as a result of aluminum-matrix decomposition in the course of thermomechanical treatment. For example, the structure of the as-hot-rolled CMSZ specimen contains subgrains elongated in the deformation direction. The dislocations are arranged randomly, with their density being high (Figure 3a). The structure contains a large number of <100 nm sized particles well-resolvable both in bright-field (Figure 3b) and dark-field (Figure 3c) images. The particles are arranged randomly relative to the aluminum matrix and to one another, leading to the formation of diffraction rings in the electron-diffraction pattern. Most of those particles can be identified as Mn-containing dispersoids ($\text{Al}_{20}\text{Cu}_2\text{Mn}_3$ and $\text{Al}_{15}\text{Mn}_2\text{Si}_3$); however, analysis of the diffraction pattern proved some of them to be Al_3Zr particles.

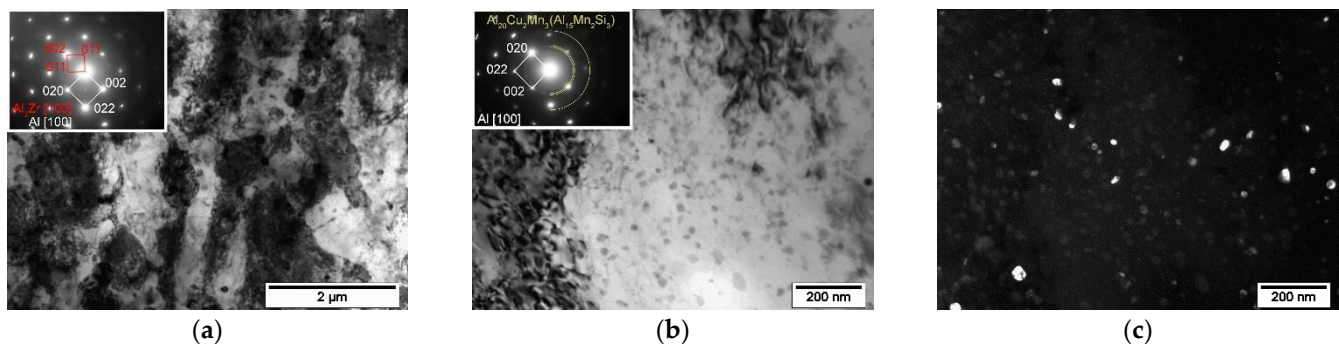


Figure 3. TEM images in (a,b) bright-field and (c) dark-field of CMSZ alloy in HR condition, (a,b) with corresponding diffraction patterns.

The structure of the test alloy processed following the A350-6 regime (Figure 4) differs but only slightly from the structure of the as-hot-rolled alloy, except for the absence of a clearly pronounced rolling structure. One can also see a large number of <100 nm sized Mn- and Zr-containing particles which segregate at subgrain boundaries (Figure 4b), thus hindering boundary migration and, therefore, stabilizing the structure of the material at high operation temperatures.

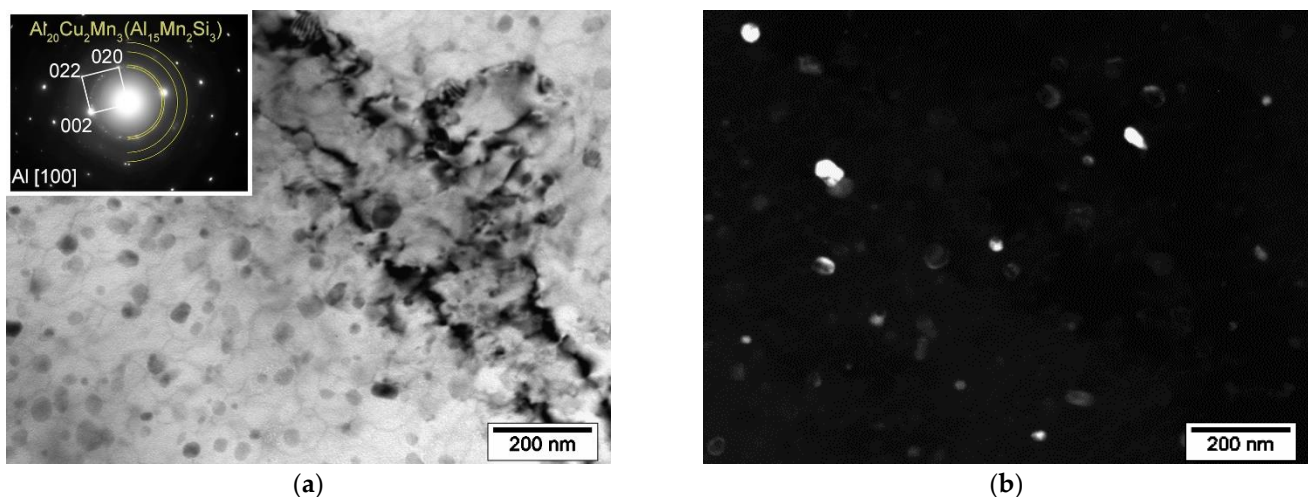


Figure 4. TEM images in (a) bright-field and (b) dark-field of CMSZ alloy in A350-6 condition, (a) with corresponding diffraction pattern.

By way of comparison, Figure 5a,b shows the typical structure of the artificially aged 2219 alloy. Both images indicate the precipitation of θ' phase particles along the {001} planes of α -aluminum, which is typical of the alloy in this state. The size of the particles is 40–60 nm, with their boundaries being semi-coherent. Some inclusions are markedly larger than others, with their orientation differing in some cases (Figure 5b) from that of the other particles. Those inclusions can be identified as the θ phase arranging incoherently relative to the aluminum matrix, and, therefore, their orientation differs from that of the θ' phase particles.

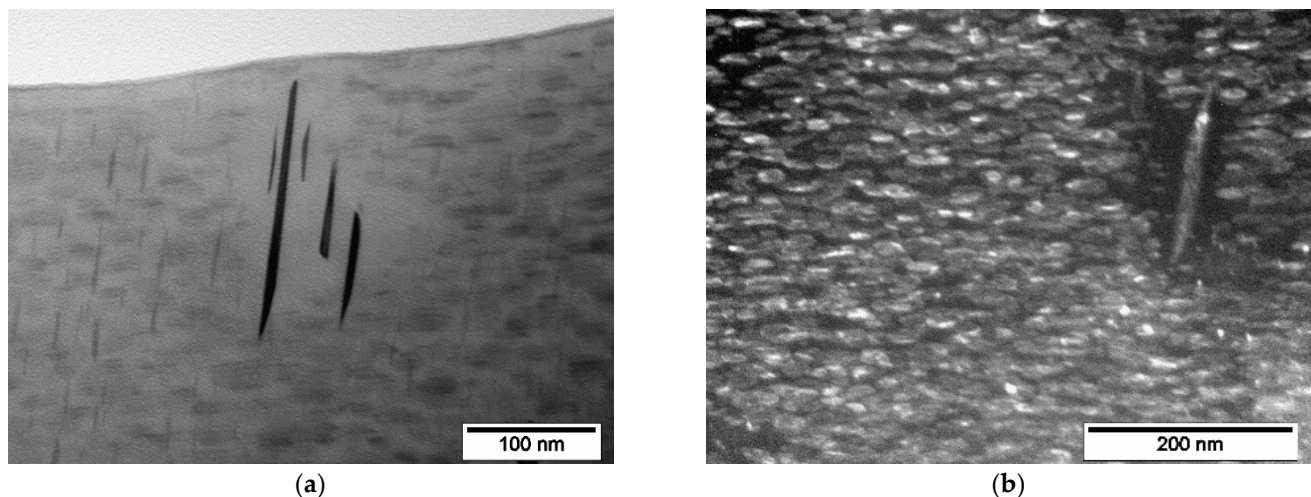


Figure 5. TEM images in (a) bright-field and (b) dark-field of 2219 alloy in AA condition.

3.3. Mechanical Properties

Figure 6 illustrates the change in the microhardness of the specimens processed using the regimes summarized in Table 2. The hot-deformed 2219 alloy exhibits slight deformation hardening. The hot-deformed and annealed 2219 alloy undergoes reverse (recrystallization) processes and inner stress relaxation, leading to softening. Quenching noticeably increases the hardness and reduces the electrical conductivity due to copper dissolution in the aluminum matrix and the formation of a supersaturated Al. The hardness of the artificially aged 2219 alloy is the highest, reaching 146 HV¹ (Figure 6a). It should be noted that deformation treatment immediately before artificial aging did not affect HV. After long-term high-temperature exposure, the microhardness of the 2219 alloy specimen decreased dramatically to 63 HV¹ due to coarsening of the predominant θ' phase in the alloy.

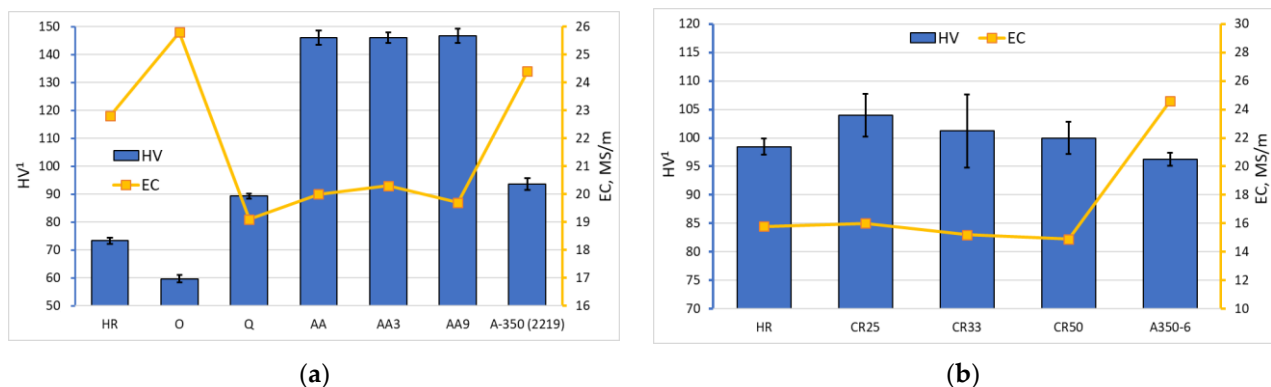


Figure 6. HV and EC of (a) 2219 and (b) CMSZ alloys.

The hardness of the CMSZ alloy after different types of deformation and heat treatment is more uniform (Figure 6b). The hardness of the HR-CMSZ specimen is 99 HV¹. As described above, this hardness is achieved due to the formation of a subgrain structure with a large number of dispersoids as a result of deformation. Cold rolling of the specimen slightly increases the hardness due to deformation hardening. This fact indicates a low deformation, strengthening susceptibility of the alloy. It is more important, however, that annealing does not affect the hardness of the alloy. Indeed, 6 h 350 °C heat treatment reduced the microhardness of the specimens by an average of 4 HV¹ in comparison with the CR50 condition, confirming the high thermal stability of the CMSZ alloy.

Figure 6 also shows electrical conductivity data. EC and its variations are known to be in good agreement with the heat conductivity and microstructural changes of materials, e.g., phase transformations [16]. The EC of the 2219 alloy is the highest after hot rolling and annealing due to the depletion of the aluminum solid solution after these treatments. Quenching reduces the EC of the alloy to 19 MS/m due to Cu dissolution in (Al). Aging (AA, AA3 and AA9) increases the conductivity of the alloy by an average of 1 MS/m due to the decomposition of the solid solution and the formation of the θ' phase. The deformed CMSZ alloy specimens typically exhibit slight changes in the EC. The electrical conductivity of the hot-rolled specimen is controlled by the Mn content in (Al). Cold rolling with different deformation degrees causes a variation of the EC within the confidence interval due to defect formation in the crystal structure of the specimens. Further decomposition of the as-annealed aluminum solid solution in the A350-6 specimen leads to a significant growth of the EC to 24.6 MS/m.

The most interesting tear test data for the specimens are shown in Figure 7 and are summarized in Table 3. By and large, the YS and UTS figures are in agreement with the microhardness data as can be seen from the diagram. The 2219 commercial alloy specimen subjected to the conventional deformation and heat-treatment route had the best mechanical properties meeting the performance requirements for it. The hot-rolled and annealed CMSZ alloy specimens exhibit moderate but almost stable properties regardless of cold deformation or high-temperature treatment. Cold rolling leads to a slight increase in the yield strength and an appropriate decrease in the hardness which, nevertheless, remains sufficiently high. On the contrary, subsequent high-temperature annealing at 350 °C for 6 h completely recovers the properties achieved after hot rolling. One can, therefore, conclude that the new alloy exhibits an excellent thermal stability which becomes evident when compared with grade 2219 alloy after similar annealing. Indeed, one can see from Table 3 that similar annealing of the grade alloy reduces its yield strength twofold, to about 1.5 times lower than that of the new model alloy.

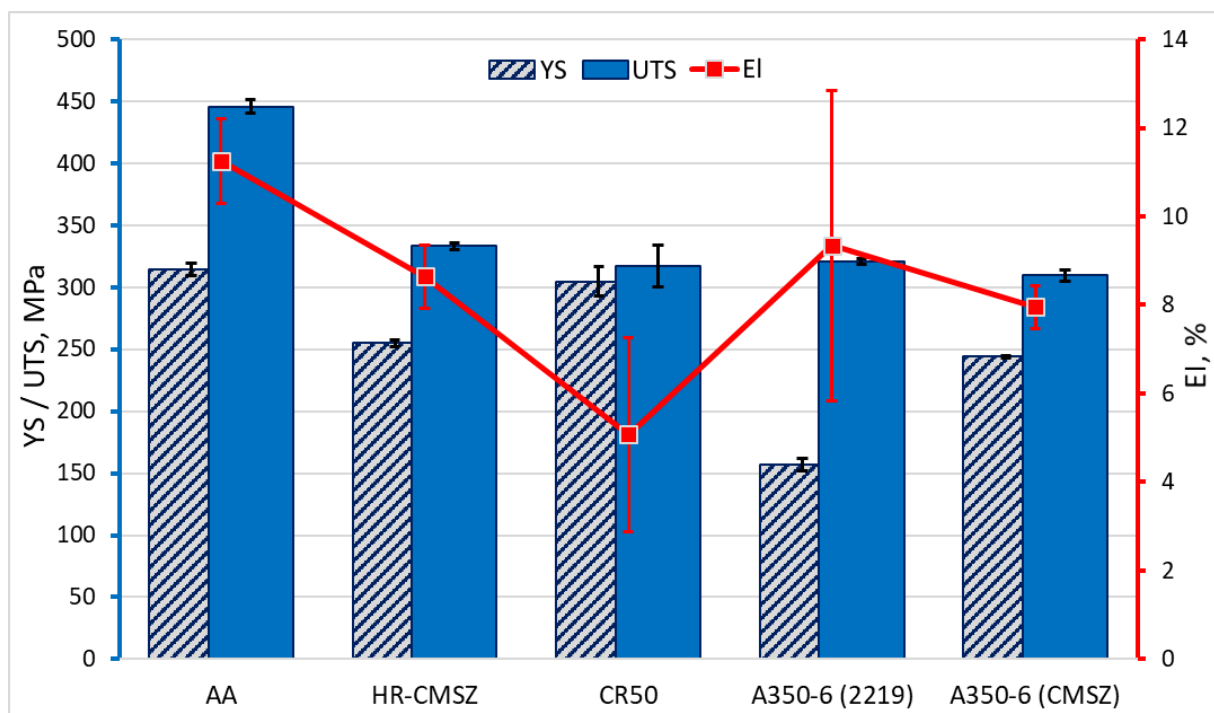


Figure 7. Yield strength (YS), ultimate tensile strength (UTS), and elongation (EI) of experimental alloys.

Table 3. Mechanical properties of experimental alloys.

| Alloy | Route | HV | | YS, MPa | | UTS, MPa | | El, % | |
|-------|--------|-------|-----|---------|------|----------|------|-------|-----|
| | | Value | sd | sd | sd | Value | sd | sd | sd |
| 2219 | AA | 146 | 2.6 | 314 | 4.8 | 446 | 5.3 | 11.3 | 0.9 |
| | A350-6 | 63 | 2.0 | 157 | 4.6 | 320 | 2.4 | 9.3 | 3.5 |
| CMSZ | HR | 99 | 1.4 | 255 | 3.1 | 333 | 2.9 | 8.6 | 0.7 |
| | CR50 | 100 | 2.8 | 305 | 11.9 | 317 | 16.9 | 5.1 | 2.2 |
| | A350-6 | 96 | 1.1 | 244 | 1.4 | 309 | 4.3 | 7.9 | 0.5 |

3.4. Discussion

The alloys studied in this work pertain to different groups of aluminum alloys. The 2219 alloy is heat-treatable, and increasing its strength and plasticity requires additional quenching and aging steps in its process route. The experimental CMSZ alloy is a non-heat-treatable one. Experimental results also indicate a low deformation hardening susceptibility of this alloy composition. Thus, alloying processes and deformation–heat-treatment modes deliver the main contribution to the properties of the CMSZ alloy. These operations provide for the formation of fine-grained manganese- and zirconium-containing particles (Al_{20} , Al_{15} and Al_3) in the structure of rolled sheets, with these particles being the main factor delivering the high thermal stability of the test alloy.

Results of quantitative analysis of the fraction of phases and composition of Al for the experimental alloys (based on their actual compositions (Table 1)) at 350 °C are summarized in Table 4. The data show that the equilibrium concentrations of Cu, Mn, Si, and Zr in Al are the same for both alloys. Calculations showed that the AA2219 and CMSZ alloys contain approximately equal total fractions of the excess phases (Al_2Cu , $\text{Al}_{20}\text{Cu}_2\text{Mn}_3$, $\text{Al}_{15}\text{Mn}_2\text{Si}_3$, and Al_3Zr). The calculations also showed that the CMSZ model alloy contains a high amount of the $\text{Al}_{20}\text{Cu}_2\text{Mn}_3$ and $\text{Al}_{15}\text{Mn}_2\text{Si}_3$ phases (about 3 and 4.6 wt.%, respectively). However, the Al_2Cu phase dominates in the 2219 alloy.

Table 4. Calculated phase composition of experimental alloys at 350 °C.

| Alloy | Fraction of Phase, wt.% | | | | | Concentration in (Al), wt.% | | | |
|-------|-------------------------|------------------|------------------|------------------------|-------|-----------------------------|------|-------------|------|
| | Al_2Cu | Al_{20} | Al_{15} | Al_3Zr | (Al) | Cu | Mn | Si | Zr |
| 2219 | 9.60 | 1.76 | - | 0.58 | 88.05 | 0.86 | 0.02 | ≤ 0.01 | 0.07 |
| CMSZ | 1.35 | 3.03 | 4.58 | 0.20 | 90.83 | 0.86 | 0.02 | 0.02 | 0.07 |

The properties of the grade heat-treatable 2219 alloy in the AA condition are in a very good agreement with the standard requirements to the alloy in the T6 condition, and the resultant microstructure being typical of that alloy. The large quantity of ordered θ' phase particles in the alloy structure favor its high strength and plasticity. The selected artificial-aging regime provides for the optimum combination of properties that are superior to the YS and El parameters for artificially aged specimens obtained earlier [33]. A combination of preliminary hot deformation (5 and 10%) and artificial aging (Figure 8, CPD + AA) allowed for the achievement of a higher strength at a lower plasticity. The hardness and electrical conductivity data (Figure 6a—AA3 and AA9) suggest that preliminary cold deformation before aging has but a little effect ranging within standard statistical deviation. However, despite the substantially higher strength, the predominant fraction of the metastable θ' phase makes this chemical composition and processing route of the alloy unsuitable for high-temperature operation. It was reported [16] that even short-term operation at 250 °C leads to a degradation of 2219 alloy properties to the level of Al-2Cu-2Mn, and operation at 300 °C further impairs the alloy properties (Figure 8, AA + A-300). The data presented in

this work confirm earlier results, showing a reduction of 2219 alloy's YS of four times and an El reduction of 2% after 6 h 350 °C heat treatment (Figure 8, AA + A-350).

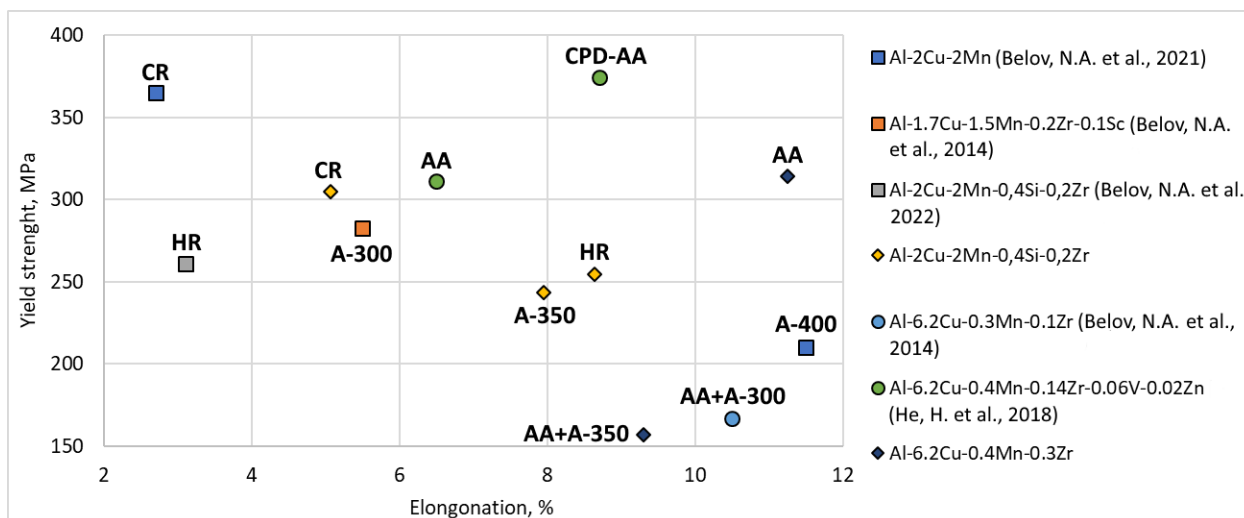


Figure 8. Comparison of mechanical properties of Al-Cu-Mn system alloys according to experimental data and data from other sources [11,16,31,33].

The large number of <100 nm sized nanostructural particles forming in the CMSZ alloy upon hot deformation provide for efficient structural stabilization. Indeed, as can be seen from microstructural images, the large quantity of the $\text{Al}_{15}\text{Mn}_2\text{Si}_3$ and Al_3Zr phase particles and the absence of secondary Al_2Cu particles favor the preservation of the predominantly deformed CMSZ alloy structure even after long-term high-temperature treatment. YS and El data for this system alloys reported elsewhere (Figure 8) suggest a substantially predetermined strength level of within 300–350 MPa and the possibility of controlling the plasticity of the alloys over a wide range. The effect of annealing at 300 to 400 °C (Figure 8, A-300 and A-400, respectively) can be clearly seen in the slight reduction of YS from 283 to 210 MPa and the gradual linear growth of El by 5%. As was concluded earlier [16], increasing the strength of Al-Cu-Mn system alloys requires reducing the size of the $\text{Al}_{20}\text{Cu}_2\text{Mn}_3$ dispersoids or increasing their content in the material. Zirconium and silicon microalloying aimed to form thermally stable phases, coupled with a lower hot rolling temperature (400 °C) and a higher deformation rate at final rolling passes, provide for the best combination of strength and plasticity (Figure 8, yellow rhomb–HR) in comparison with the other experimental results. YS, in this case, totaled 255 MPa, and El is 8.6%. One should also bear in mind that earlier data [11] (Figure 8, A-300) demonstrate quite a small effect of Sc microalloying on the thermal stability of the Al-Cu-Mn system alloy, i.e., that this alloying is unnecessary.

Thus, the experimental results allowed for finding the optimum deformation and temperature for flat rolling of the thermally stable CMSZ (Al-2%Cu-2%Mn-0.4%Si-0.2%Zr) alloy exhibiting high processability in comparison with other 2xxx system alloys, e.g., the heat-treatable 2219 one, without expensive alloying additions.

4. Conclusions

1. The phase composition, microstructure, and mechanical properties of non-heat-treatable experimental Al-2%Cu-2%Mn-0.4%Si-0.2%Zr alloy rolled sheets were studied after different deformation and heat-treatment modes and the data were compared with those for the graded heat-treatable AA2219 alloy;
2. The as-cast structure of the experimental alloys (except for the Al_2Cu phase) contains a small quantity of eutectic phase inclusions and Mn-containing phase interlayers at dendrite cell boundaries that favor the deformability and processability of the alloy;

3. The microstructures of the as-deformed experimental alloy specimens and the long-term high-temperature-treated ones contain multiple nanosized Mn- and Zn-containing particles (Al_{20} , Al_{15} , Al_3Zr) that deliver the major contribution to the thermal stability of the alloy;
4. The 3 to 9% pre-aging deformation of the 2219 heat-treatable alloy specimens had but a little effect on the properties of the rolled sheets. The aged rolled sheets have high YS and UTS (314 and 446 MPa, respectively) which, however, decrease noticeably upon heat treatment at above 250–270 °C;
5. The room-temperature mechanical properties of the model non-heat-treatable alloy were studied: The UTS and YS parameters of the hot-rolled CMSZ alloy are 333 and 255 MPa, respectively, the relative elongation being –8.6%. These parameters are the highest for the test alloy and confirm that achieving its best properties does not require additional processing. At 6 h 350 °C heat treatment of the alloy reduces its mechanical properties but slightly;
6. Zr and Si microalloying and use of the herein-suggested process route for rolling of semi-finished rolled sheets of the Al-Cu-Mn system alloy prove to deliver the best final product performance that is superior to results achieved in earlier works and to the thermal stability of the compared graded alloy.

Author Contributions: Conceptualization: A.K.; data analysis: S.C. and Y.G.; data interpretation: A.K. and A.F.; experiment: A.K., S.C. and Y.G.; writing—original draft preparation: A.K.; writing—review and editing: A.F. and A.C. All authors have read and agreed to the published version of the manuscript.

Funding: This work was financially supported by the Moscow Polytechnic University within the framework of the grant named after Pyotr Kapitsa.

Data Availability Statement: Data are contained within the article.

Conflicts of Interest: The authors declare no conflict of interest.

References

1. Kammer, C. Aluminum and Aluminum Alloys. In *Springer Handbook of Materials Data*; Springer Handbooks; Warlimont, H., Martienssen, W., Eds.; Springer: Cham, Switzerland, 2018; pp. 161–197.
2. Davis, J.R. Aluminum and Aluminum Alloys. In *ASM Specialty Handbook*; ASM International: Novelt, OH, USA, 1993.
3. Ber, L.B.; Kolobnev, N.I.; Tsukrov, S.L. *Heat Treatment of Aluminum Alloys*, 1st ed.; CRC Press: Boca Raton, FL, USA, 2020.
4. Fine, M.E. Precipitation Hardening of Aluminum Alloys. *Metall. Trans. A* **1975**, *6*, 625–630. [\[CrossRef\]](#)
5. Sanders, R.; Staley, J.T. *History of Wrought Aluminum Alloys and Applications, Volume 2B: Properties and Selection of Aluminum Alloys*; ASM International: Novelt, OH, USA, 2019.
6. Mondolfo, L.F. *Aluminum Alloys: Structure and Properties*, 1st ed.; Butterworth-Heinemann: London, UK, 1976.
7. Belov, N.A.; Eskin, D.G.; Aksenov, A.A. *Multicomponent Phase Diagrams: Applications for Commercial Aluminum Alloys*, 1st ed.; Elsevier Science: Amsterdam, The Netherlands, 2005.
8. Zhang, Y.; Li, R.; Chen, P.; Li, X.; Liu, Z. Microstructural evolution of Al_2Cu phase and mechanical properties of the large-scale Al alloy components under different consecutive manufacturing processes. *J. Alloys Compd.* **2019**, *808*, 151634. [\[CrossRef\]](#)
9. Wan, S.; Su, H.; Shao, B.; Zong, Y.; Shan, D.; Guo, B. Changes in microstructure and mechanical properties of 2219 Al alloy during hot extrusion and post-extrusion aging. *J. Mater. Res. Technol.* **2023**, *24*, 3453–3463. [\[CrossRef\]](#)
10. Mao, X.; Yi, Y.; He, H.; Huang, S.; Guo, W. Second phase particles and mechanical properties of 2219 aluminum alloys processed by an improved ring manufacturing process. *Mater. Sci. Eng. A* **2020**, *781*, 139226. [\[CrossRef\]](#)
11. Belov, N.A.; Alabin, A.N.; Matveeva, I.A. Optimization of phase composition of Al–Cu–Mn–Zr–Sc alloys for rolled products without requirement for solution treatment and quenching. *J. Alloys Compd.* **2014**, *583*, 206–213. [\[CrossRef\]](#)
12. Akopyan, T.K.; Letyagin, N.V.; Belov, N.A.; Fortuna, A.S.; Nguen, X.D. The role of Sn trace addition in the precipitation behavior and strengthening of the wrought Al–Cu–Mn-based alloy. *J. Mater. Sci.* **2023**, *58*, 8210–8229. [\[CrossRef\]](#)
13. Chen, B.A.; Pan, L.; Wang, R.H.; Liu, G.; Cheng, P.M.; Xiao, L.; Sun, J. Effect of solution treatment on precipitation behaviors and age hardening response of Al–Cu alloys with Sc addition. *Mater. Sci. Eng. A* **2011**, *530*, 607–617. [\[CrossRef\]](#)
14. Tiryakioğlu, M.; Shuey, R.T. Quench sensitivity of 2219-T87 aluminum alloy plate. *Mater. Sci. Eng. A* **2010**, *527*, 5033–5037. [\[CrossRef\]](#)
15. Dar, S.M.; Liao, H. Creep behavior of heat resistant Al–Cu–Mn alloys strengthened by fine (θ') and coarse ($\text{Al}_{20}\text{Cu}_2\text{Mn}_3$) second phase particles. *Mater. Sci. Eng. A* **2019**, *763*, 138062. [\[CrossRef\]](#)

16. Belov, N.A.; Akopyan, T.K.; Shurkin, P.K.; Korotkova, N.O. Comparative analysis of structure evolution and thermal stability of commercial AA2219 and model Al-2 wt%Mn-2 wt%Cu cold rolled alloys. *J. Alloys Compd.* **2021**, *864*, 158823. [\[CrossRef\]](#)
17. Dorin, T.; Ramajayam, M.; Lamb, J.; Langan, T. Effect of Sc and Zr Additions on the Microstructure/Strength of Al–Cu Binary Alloys. *Mater. Sci. Eng. A* **2017**, *707*, 58–64. [\[CrossRef\]](#)
18. Kairy, S.K.; Rouxel, B.; Dumbre, J.; Lamb, J.; Langan, T.J.; Dorin, T.; Birbilis, N. Simultaneous Improvement in Corrosion Resistance and Hardness of a Model 2xxx Series Al–Cu Alloy with the Microstructural Variation Caused by Sc and Zr. *Corros. Sci.* **2019**, *158*, 108095. [\[CrossRef\]](#)
19. Gao, Y.H.; Yang, C.; Zhang, J.Y.; Cao, L.F.; Liu, G.; Sun, J.; Ma, E. Stabilizing Nanoprecipitates in Al–Cu Alloys for Creep Resistance at 300 °C. *Mater. Res. Lett.* **2019**, *7*, 18–25. [\[CrossRef\]](#)
20. Rouxel, B.; Ramajayam, M.; Langan, T.J.; Lamb, J.; Sanders, P.G.; Dorin, T. Effect of Dislocations, Al₃(Sc, Zr) Distribution and Ageing Temperature on θ' Precipitation in Al–Cu–(Sc)–(Zr) Alloys. *Materialia* **2020**, *9*, 100610. [\[CrossRef\]](#)
21. Lamb, J.; Rouxel, B.; Langan, T.; Dorin, T. Novel Al–Cu–Mn–Zr–Sc Compositions Exhibiting Increased Mechanical Performance after a High-Temperature Thermal Exposure. *J. Mater. Eng. Perform.* **2020**, *29*, 5672–5684. [\[CrossRef\]](#)
22. Amer, S.M.; Barkov, R.Y.; Prosviryakov, A.S.; Pozdniakov, A.V. Structure and Properties of New Wrought Al–Cu–Y- and Al–Cu–Er-Based Alloys. *Phys. Met. Metallogr.* **2021**, *122*, 915–922. [\[CrossRef\]](#)
23. Amer, S.M.; Mamzurina, O.I.; Loginova, I.S.; Glavatskikh, M.V.; Barkov, R.Y.; Pozdniakov, A.V. Effect of Mn Addition on the Phase Composition and Strengthening Behavior of AlCuYbZr and AlCuGdZr Alloys. *JOM* **2022**, *74*, 3646–3654. [\[CrossRef\]](#)
24. Mikhaylovskaya, A.V.; Kotov, A.D.; Barkov, R.Y.; Yakovtseva, O.A.; Glavatskikh, M.V.; Loginova, I.S.; Pozdniakov, A.V. The Influence of Y and Er on the Grain Structure and Superplasticity of Al–Cu–Mg–Based Alloys. *JOM* **2023**. [\[CrossRef\]](#)
25. Vlach, M.; Stulikova, I.; Smola, B.; Piesova, J.; Cisarova, H.; Danis, S.; Plasek, J.; Gemma, R.; Tanprayoon, D.; Neubert, V. Effect of cold rolling on precipitation processes in Al–Mn–Sc–Zr alloy. *Mater. Sci. Eng. A* **2012**, *548*, 27–32. [\[CrossRef\]](#)
26. Belov, N.A.; Alabin, A.N. Energy Efficient Technology for Al–Cu–Mn–Zr Sheet Alloys. *Mater. Sci. Forum* **2013**, *765*, 13–17. [\[CrossRef\]](#)
27. Dorin, T.; Ramajayam, M.; Vahid, A.; Langan, T. Chapter 12—Aluminium Scandium Alloys. In *Fundamentals of Aluminium Metallurgy. Recent Advances*; Lumley, R.N., Ed.; Woodhead Publishing: Sawston, UK, 2018; pp. 439–494.
28. Yashin, V.V.; Aryshenskii, E.V.; Drita, A.M.; Grechnikov, F.V.; Ragazin, A.A.; Bazhenov, V.E. Effect of Scandium on the Microstructure of the Al–Cu–Mn–Mg–Hf–Nb Alloy. *Phys. Met. Metallogr.* **2021**, *122*, 960–968. [\[CrossRef\]](#)
29. Belov, N.A.; Avksent'eva, N.N. Quantitative Analysis of the Al–C–Mg–Mn–Si Phase Diagram as Applied to Commercial Aluminum Alloys of Series 2xxx. *Met. Sci. Heat. Treat.* **2013**, *55*, 358–363. [\[CrossRef\]](#)
30. Belov, N.A.; Cherkasov, S.O.; Korotkova, N.O.; Yakovleva, A.O.; Tsydenov, K.A. Effect of Iron and Silicon on the Phase Composition and Microstructure of the Al-2% Cu-2% Mn (wt %) Cold Rolled Alloy. *Phys. Met. Metallogr.* **2021**, *122*, 1095–1102. [\[CrossRef\]](#)
31. Belov, N.A.; Tsydenov, K.A.; Letyagin, N.V.; Cherkasov, S.O. Structure and mechanical properties of hot rolled sheets of Al-2% Cu-2% Mn-0.4% Si-0.2% Zr alloy subjected to friction stir welding. *Tsvetnye Met.* **2022**, *5*, 66–72. [\[CrossRef\]](#)
32. Belov, N.A.; Akopyan, T.K.; Korotkova, N.O.; Cherkasov, S.O.; Yakovleva, A.O. Effect of Fe and Si on the Phase Composition and Microstructure Evolution in Al-2 wt.% Cu-2 wt.% Mn Alloy During Solidification, Cold Rolling and Annealing. *JOM* **2021**, *73*, 3827–3837. [\[CrossRef\]](#)
33. He, H.; Yi, Y.; Huang, S.; Zhang, Y. Effects of cold predeformation on dissolution of second-phase Al₂Cu particles during solution treatment of 2219 Al–Cu alloy forgings. *Mater. Charact.* **2018**, *135*, 18–24. [\[CrossRef\]](#)

Disclaimer/Publisher's Note: The statements, opinions and data contained in all publications are solely those of the individual author(s) and contributor(s) and not of MDPI and/or the editor(s). MDPI and/or the editor(s) disclaim responsibility for any injury to people or property resulting from any ideas, methods, instructions or products referred to in the content.